Comparing tonic and phasic calcium in the dendrites of vulnerable midbrain neurons

Rita Chen[1] and Rebekah Evans[1]

[1]Georgetown University Medical Center

August 29, 2023

Abstract

Several midbrain nuclei degenerate in Parkinson's Disease. Many of these nuclei share the common characteristics that are thought to contribute to their selective vulnerability, including pacemaking activity and high levels of calcium influx. In addition to the well-characterized dopaminergic neurons of the substantia nigra pars compacta (SNc), the cholinergic neurons of the pedunculopontine nucleus (PPN) also degenerate in PD. It is well established that the low-threshold L-type calcium current is a main contributor to tonic calcium in SNc dopaminergic neurons and is hypothesized to contribute to their selective vulnerability. However, it is not yet clear whether the vulnerable PPN cholinergic neurons share this property. Therefore, we used two-photon dendritic calcium imaging and whole-cell electrophysiology to evaluate the role of L-type calcium channels in the tonic and phasic activity of PPN neurons and the corresponding dendritic calcium signal and directly compare these characteristics to SNc neurons. We found that blocking L-type channels reduces tonic firing rate and dendritic calcium levels in SNc neurons. By contrast, the calcium load in PPN neurons during pacemaking did not depend on L-type channels. However, we find that blocking L-type channels reduces phasic calcium influx in PPN dendrites. Together, these findings show that L-type calcium channels play different roles in the activity of SNc and PPN neurons, and suggest that low-threshold L-type channels are not responsible for tonic calcium levels in PPN cholinergic neurons and are therefore not likely to be a source of selective vulnerability in these cells.

1 **Comparing tonic and phasic calcium in the dendrites of vulnerable**

2 **midbrain neurons**

3

4 Authors: Dr. Rita Yu-Tzu Chen[1], Dr. Rebekah C. Evans[1*]

5

6 [1] Department of Neuroscience, Georgetown University Medical Center, Washington

7 DC

8

9 *Corresponding author

10 Dr. Rebekah C. Evans

11 Department of Neuroscience

12 Georgetown University Medical Center

13 3970 Reservoir Rd NW

14 New Research Building

15 Washington DC, USA 20057

16 re285@georgetown.edu

17

18 Running Title: Dendritic calcium in vulnerable neurons

19

20 Author Contributions: R.C.E. and R.Y-T.C. conceived of the project and planned the

21 experiments. R.Y-T.C. performed the experiments, analyzed the data, made the

22 figures, and wrote the manuscript. R.C.E. and R.Y-T.C. edited and revised the

23 manuscript.

24

25 Conflict of Interest statement: The authors have no conflicts of interest.

26

27 Data availability statement: Data will be made available upon request.

28

35

36 Abstract

37

38 Several midbrain nuclei degenerate in Parkinson's Disease. Many of these nuclei

39 share the common characteristics that are thought to contribute to their selective

40 vulnerability, including pacemaking activity and high levels of calcium influx. In

41 addition to the well-characterized dopaminergic neurons of the substantia nigra pars

42 compacta (SNc), the cholinergic neurons of the pedunculopontine nucleus (PPN) also

43 degenerate in PD. It is well established that the low-threshold L-type calcium current

44 is a main contributor to tonic calcium in SNc dopaminergic neurons and is

45 hypothesized to contribute to their selective vulnerability. However, it is not yet clear

46 whether the vulnerable PPN cholinergic neurons share this property. Therefore, we

47 used two-photon dendritic calcium imaging and whole-cell electrophysiology to

48 evaluate the role of L-type calcium channels in the tonic and phasic activity of PPN

49 neurons and the corresponding dendritic calcium signal and directly compare these

50 characteristics to SNc neurons. We found that blocking L-type channels reduces tonic

51 firing rate and dendritic calcium levels in SNc neurons. By contrast, the calcium load

52 in PPN neurons during pacemaking did not depend on L-type channels. However, we

53 find that blocking L-type channels reduces phasic calcium influx in PPN dendrites.

54 Together, these findings show that L-type calcium channels play different roles in the

55 activity of SNc and PPN neurons, and suggest that low-threshold L-type channels are

56 not responsible for tonic calcium levels in PPN cholinergic neurons and are therefore

57 not likely to be a source of selective vulnerability in these cells.

58

Introduction

Parkinson's disease (PD) is a disabling neurodegenerative disease characterized by motor deficits such as bradykinesia and rigidity, as well as cognitive decline (Poewe et al., 2017). The cardinal symptoms of PD have been attributed to loss of dopaminergic neurons in the substantia nigra pars compacta (SNc), but several other brainstem nuclei also degenerate (Braak et al., 2004; Giguère et al., 2018). Of particular interest, ~30-60% of cholinergic pedunculopontine nucleus (PPN) neurons are lost in PD patients (Giguère et al., 2018; Jellinger, 1988; Rinne et al., 2008; Sébille et al., 2019). PPN cholinergic neurons directly innervate motor structures in the basal ganglia and lower brainstem (Mena-Segovia and Bolam, 2017), and their degeneration may contribute to gait and balance impairments (Chambers et al., 2021; Grabli et al., 2013; Karachi et al., 2010; Rinne et al., 2008). However, it is not known why PPN cholinergic neurons and SNc dopaminergic neurons selectively degenerate in PD.

The factors that make some neurons vulnerable to degeneration while others are resilient have been elusive. While there are multiple hypotheses for selective vulnerability (Giguère et al., 2018; Gonzalez-Rodriguez et al., 2020), one of particular therapeutic interest is that tonic pacemaking and the accompanying calcium (Ca^{2+}) influx increases neural vulnerability. The pacemaking activity of SNc dopaminergic neurons is well characterized (Grace and Onn, 1989; Johnson et al., 1992). It is accompanied by large somatodendritic Ca^{2+} oscillations primarily mediated by low-threshold L-type Ca^{2+} channels (Chan et al., 2007; Guzman et al., 2009; Hage and Khaliq, 2015; Shin et al., 2022). Because this chronic Ca^{2+} load adds to metabolic cost (Surmeier et al., 2010) and contributes to mitochondrial oxidative stress (Dryanovski et al., 2013; Guzman et al., 2010), L-type Ca^{2+} channel blockers have been investigated as treatment to slow the progress of PD in animal models (Liss and Striessnig, 2019; Ortner, 2021) and in clinical trials (Parkinson Study Group STEADY-PD III Investigators, 2020; Surmeier et al., 2022).

PPN cholinergic neurons, like SNc dopaminergic neurons, spontaneously fire action potentials in the absence of excitatory synaptic input (Takakusaki and Kitai, 1997).

3

92 However, it is not known whether this tonic pacemaking contributes to their

93 vulnerability in PD or whether they share pacemaking mechanisms with the

94 vulnerable SNc dopaminergic neurons. Previous studies indicate that PPN cholinergic

95 neurons undergo Ca^{2+}-dependent membrane potential oscillations (Hyde et al., 2013;

96 Kezunovic et al., 2011; Takakusaki and Kitai, 1997), but dendritic Ca^{2+} activity during

97 pacemaking has not yet been measured. To determine whether PPN cholinergic

98 neurons share the same pacemaking and Ca^{2+} influx mechanisms as SNc

99 dopaminergic neurons, we used whole-cell patch clamp with simultaneous two-

100 photon Ca^{2+} imaging to measure dendritic Ca^{2+} during tonic and phasic action

101 potential firing. We find that PPN cholinergic neurons exhibit pacemaking Ca^{2+} that is

102 highly associated with action potential spiking, but unlike SNc neurons, this tonic Ca^{2+}

103 is not mediated by L-type channels. However, we find that L-type channels contribute

104 to phasic firing-induced Ca^{2+} entry in PPN neurons, suggesting that they express high-

105 threshold L-type channels. Therefore, these findings reveal that L-type channels play

106 different roles in the regulation of tonic and phasic Ca^{2+} dynamics in PPN and SNc

107 neurons, and show that PPN cholinergic neurons do not rely on low-threshold L-type

108 channels for spontaneous pacemaking or tonic Ca^{2+} levels.

109

Methods

Animals

All animal procedures were approved by the Georgetown University Medical Center
Institutional Animal Care and Use Committee (IACUC). ChAT-Cre (strain #031661) and
Ai9/tdTomato (strain #007909) mice on the C57BL/6J background were purchased
from Jackson Laboratory and crossed to produce ChAT-Cre/TdTomato mice. WT
C57BL/6J (strain #000664) mice were purchased from Jackson Laboratory and bred in
the Georgetown University Department of Comparative Medicine animal facility.
Mice were group-housed with same-sex littermates when possible and had *ad
libitum* access to food and water in a 12-hr light/12-hr dark cycle room.

Slice preparation

Horizontal brain slices (200 μm) were prepared from adult ChAT-Cre/tdTomato or WT
mice of either sex (>2 months old, average age = 110 ± 5 days, range = 70-140 days).
Mice were anesthetized with isoflurane and transcardially perfused with ice-cold
slicing solution containing (in mM): 198 glycerol, 25 $NaHCO_3$, 2.5 KCl, 1.2 NaH_2PO_4, 20
HEPES, 10 glucose, 10 $MgCl_2$, 0.5 $CaCl_2$ (bubbled with 95% O_2/5% CO_2, osmolarity =
310-320 mmol/kg). Brains were then quickly extracted and slices were prepared
using Leica VT1200S vibratome in the same slicing solution. The slices were
transferred to and incubated for 30 min in a heated (34 °C) modified ACSF containing
(in mM): 92 NaCl, 30 $NaHCO_3$, 2.5 KCl, 1.2 NaH_2PO_4, 20 HEPES, 35 glucose, 2 $MgCl_2$, 2
$CaCl_2$, 5 Na-ascorbate, 3 Na-pyruvate, 2 thiourea (bubbled with 95% O_2/5% CO_2,
osmolarity = 300-310 mmol/kg). After incubation, slices were moved to room
temperature for at least an additional 30 min before recording.

Electrophysiology

Slice were transferred to a recording chamber with constant perfusion of warm (30-
34 °C) ACSF containing (in mM): 125 NaCl, 25 $NaHCO_3$, 3.5 KCl, 1.25 NaH_2PO_4, 10
glucose, 1 $MgCl_2$, 2 $CaCl_2$ (bubbled with 95% O_2/5% CO_2, osmolarity = 295-310
mmol/kg). The pedunculopontine nucleus (PPN) was identified by tdTomato
fluorescence in the ChAT+ neurons and its relative location to the superior cerebellar
peduncle and the laterodorsal tegmental nucleus. Similar numbers of ChAT+ cells

143   from the pars dissipata of rostral PPN and the pars compacta of caudal PPN were

144   sampled for each drug treatment. Dopaminergic neurons of the substantia nigra pars

145   compacta (SNc) were identified by their large soma size and relative location to the

146   medial terminal nucleus of the accessory optic tract, as well as electrophysiological

147   properties including slow pacemaking (1-8 Hz) and prominent voltage sag in

148   response to hyperpolarizing current injection.

149   Whole-cell current-clamp recordings were made with a MultiClamp 700B amplifier

150   and digitized with Digidata 1550B (Molecular Devices). Patch pipettes of tip

151   resistance 2-6 MΩ were pulled from filamented borosilicate glass and filled with the

152   intracellular solution containing (in mM): 122 $KMeSO_3$, 9 NaCl, 9 HEPES, 1.8 $MgCl_2$,

153   14 phosphocreatine, 4 Mg-ATP, 0.3 Tris-GTP, 0.05 Alexa Fluor 594, 0.3 Fluo-5F (pH =

154   7.35 with KOH; osmolarity = 290-300 mmol/kg). Current-clamp recordings were

155   bridge balanced and liquid junction potential (-8 mV) was not corrected. For analysis

156   of spontaneous tonic firing properties, only cells that were actively pacemaking were

157   included.

158

159   *Two-photon calcium imaging*

160   The majority of PPN cholinergic neurons exhibited slow pacemaking once the

161   intracellular solution dialyzed the cells. A minority of PPN neurons (15%, 4 out of 26

162   cells) remained hyperpolarized and quiescent. During Ca^{2+} imaging experiments,

163   which was initiated ≥15 min after whole-cell break-in, these 4 quiescent cells were

164   injected with a constant amount of depolarizing current to maintain stable

165   pacemaking (ranging from +30 to +120 pA). Ca^{2+} imaging was performed using

166   previously published procedures (Evans et al., 2017). Cells were imaged on a two-

167   photon microscope (Bruker) with a Mai Tai ultrafast Ti:sapphire laser (Spectra-

168   Physics) tuned to 810 nm, which activates both Alexa Fluor 594 and Fluo-5F (Sabatini

169   et al., 2002) but not tdTomato (Drobizhev et al., 2011). Linescans (2 ms lineperiod, 12

170   μs dwell time, 2 s total each scan) of the somatodendritic regions were taken at

171   512×512 pixels resolution using a 40×/0.8 NA objective (Olympus). Fluorescence

172   signals were split into red and green channels by a 575 nm dichroic long-pass mirror

173   and passed through 607/45 nm and 525/70 nm filters before being detected by

174   multi-alkali photomultiplier tubes (Bruker). To visualize cell morphology, Z-stacks (1

175   μm step, 2 or 4 μs dwell time) of each recorded cell were taken at 512×512 pixels

176 resolution after Ca^{2+} imaging experiments. Ca^{2+} signals were quantified as the ratio of

177 green to red fluorescence (G/R), normalized to the ratio of saturated green to red

178 signals (Gs/R), which were measured daily by placing a pipette filled with intracellular

179 solution plus saturating Ca^{2+} (2 mM) at the surface of the brain slice.

180

181 *Drugs*

182 All salts were from Sigma-Aldrich. Alexa Fluor 594 (Invitrogen/Life Technologies),

183 Fluo-5F (Invitrogen/Life Technologies), and tetrodotoxin-citrate (Hello Bio) were

184 dissolved in deionized water as concentrated stocks. Nifedipine (Tocris) was dissolved

185 in DMSO, stored frozen and protected from light, and thawed only once on the day of

186 use. The final concentration of DMSO in the ACSF was 0.03% (v/v) for nifedipine

187 treatment and 0.05% (v/v) for control. After baseline measurements were taken, TTX

188 was perfused in bath for 5 min and nifedipine for 8 min before post-drug

189 measurements.

190

191 *Data analysis*

192 Cell morphology and Ca^{2+} imaging data were quantified using ImageJ to determine

193 distances or fluorescence signal intensities. All numerical data including

194 electrophysiological traces were analyzed and graphed in Igor Pro (WaveMetrics).

195 The Mann-Whitney-Wilcoxon test was used to compare two unpaired samples, while

196 the Wilcoxon signed-rank test was used to compare two paired samples. The Pearson

197 correlation coefficient (r) was used to determine the significance of linear correlation

198 data. All results in text are reported as mean ± SEM. Box plots show medians as the

199 middle line, 25th and 75th percentiles as the bottom and top of the box, and 10th and

200 90th percentiles as the whiskers. Measurements from the same cell at before and

201 after conditions are linked by a line between the markers in box plots and analyzed

202 as paired data. In all figures, one asterisk (*) denotes a statistical significance level of

203 P value <0.05, two asterisks (**) P value <0.01, three asterisks (***) P value <0.001,

204 and four asterisks (****) P value <0.0001.

205

206   Results

207

208   **SNc dopaminergic and PPN cholinergic neurons differ in tonic firing properties**

209

210   The boundary of the PPN is best defined by its choline acetyltransferase (ChAT)

211   positive cholinergic neurons (Rye et al., 1987). In this study, we identified PPN

212   cholinergic neurons by red fluorescence in brain slices prepared from ChAT-tdTomato

213   transgenic mice. Dopaminergic neurons of the SNc were identified in WT or ChAT-

214   tdTomato mice by using anatomical location and electrophysiological characteristics.

215   SNc dopaminergic neurons and PPN cholinergic neurons both exhibit slow,

216   spontaneous pacemaking activity. Using two-photon laser scanning microscopy

217   combined with whole-cell patch-clamp, we visualized the dendritic morphology and

218   recorded action potentials from those two neuronal populations by filling the cells

219   with the red fluorescent dye Alexa Fluor 594.

220

221   Morphologically, SNc dopaminergic and PPN cholinergic neurons differ in soma shape

222   and the orientations of primary dendrites. The majority of SNc neurons recorded

223   have large, spindle-shaped somas (75%, 6 out of 8 cells) and primary dendrites that

224   extend parallel to the tapered ends of the soma (Fig. 1A). The average soma

225   dimensions of SNc neurons estimated from the Z-stacks are 25.38 ± 1.73 μm in

226   length and 13.89 ± 0.44 μm in width. In comparison, most PPN neurons (85%, 23 out

227   of 27 cells) have large multipolar somas with 2-4 primary dendrites coming off in

228   multiple directions (Fig. 1B), with a minority (15%, 4 out of 27 cells) having spindle-

229   shaped somas. These cholinergic neurons have an average length of 26.96 ± 0.96 μm

230   and width of 16.77 ± 0.39 μm. The membrane capacitance (Cm) of SNc and PPN

231   neurons did not differ significantly (SNc Cm: 79.18 ± 5.19 pF, n = 7; PPN Cm: 81.23 ±

232   3.44 pF, n = 26; Mann-Whitney-Wilcoxon test, p = 0.8803; Fig. 1F). However, PPN

233   neurons exhibited higher input resistance (Ri) than SNc neurons (PPN Ri: 369.7 ± 26.7

234   MΩ, n = 26; SNc Ri: 170.3 ± 23.0 MΩ, n = 7; Mann-Whitney-Wilcoxon test, p =

235   0.0004; Fig. 1G).

236

237   Both SNc dopaminergic (Grace and Onn, 1989; Johnson et al., 1992) and PPN

238   cholinergic neurons (Takakusaki and Kitai, 1997) are spontaneously active in the *ex*

239 *vivo* brain slices. In our preparation, all SNc neurons were actively firing in the cell-

240 attached configuration. In contrast, most cholinergic PPN neurons were quiescent

241 until the intracellular content was dialyzed ~2 min after obtaining the whole-cell

242 configuration. When regular pacemaking was stabilized, PPN neurons had a

243 spontaneous firing rate of 4.58 ± 0.62 Hz (n = 24), which was comparable to the rate

244 of SNc neurons at 4.48 ± 0.66 Hz (n = 8; Mann-Whitney-Wilcoxon test, p = 0.4284;

245 Fig. 1C, H). While the pacemaking of both cell types appeared robust, the

246 spontaneous firing of PPN neurons was less regular than that of SNc neurons (PPN CV

247 of ISI: 9.97 ± 1.91%, n = 24; SNc CV of ISI: 4.87 ± 0.55%, n = 8; Mann-Whitney-

248 Wilcoxon test, p = 0.0076; Fig. 1I).

249

250 Although SNc and PPN neurons did not differ in spontaneous firing rates, SNc

251 neurons exhibited significantly more depolarized membrane potential (Vm) in the

252 interspike interval than PPN neurons (SNc interspike Vm: -47.56 ± 0.39 mV, n = 8; PPN

253 interspike Vm: -56.08 ± 0.75 mV, n = 24; Mann-Whitney-Wilcoxon test, p < 0.0001;

254 Fig. 1J). When comparing the shape of action potentials (AP) (Fig. D, E), SNc neurons

255 on average had a significantly more depolarized AP threshold (SNc AP threshold: -

256 30.93 ± 0.37 mV, n = 8; PPN AP threshold: -39.34 ± 0.80 mV, n = 24; Mann-Whitney-

257 Wilcoxon test, p < 0.0001; Fig. 1K), a shorter spike height (SNc AP height: 77.65 ± 3.32

258 mV, n = 8; PPN AP height: 96.90 ± 1.51 mV, n = 24; Mann-Whitney-Wilcoxon test, p <

259 0.0001; Fig. 1L), a longer half-width (SNc AP half-width: 1.51 ± 0.17 ms, n = 8; PPN AP

260 half-width: 1.24 ± 0.04 ms, n = 24; Mann-Whitney-Wilcoxon test, p = 0.0258; Fig.

261 1M), and a shallower afterhyperpolarization trough (SNc AP trough: -55.70 ± 1.19

262 mV, n = 8; PPN AP trough: -65.10 ± 0.75 mV, n = 24; Mann-Whitney-Wilcoxon test, p <

263 0.0001; Fig. 1N). Together, these observations of spontaneous firing showed that PPN

264 cholinergic and SNc dopaminergic neurons engage in similar pacemaking activity;

265 however, the differences in average Vm, firing regularity, and AP shape suggest that

266 pacemaking may be governed by different ion channels in these two neuronal
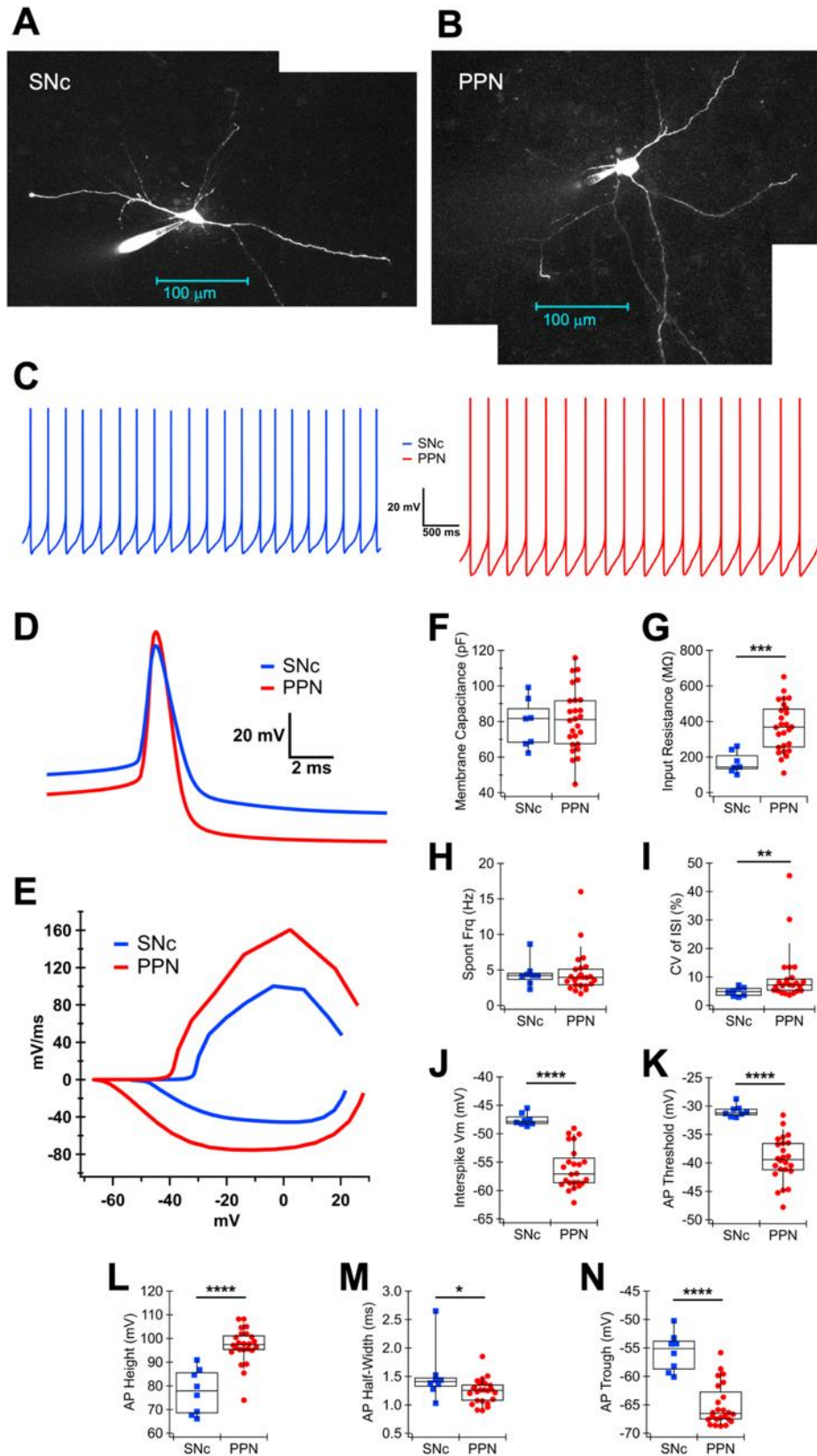
267 populations.

268

269

270

Figure 1. Electrophysiological characteristics of PPN and SNc neurons. (A)

Representative morphology of SNc dopaminergic neuron and **(B)** PPN cholinergic

273   neuron with patch pipettes visualized from maximum intensity projection of Z-stacks

274   using Alexa Fluor 594. **(C)** Representative whole-cell recordings of spontaneous

275   pacemaking of a SNc dopaminergic neuron (blue) and a PPN cholinergic neuron (red).

276   **(D)** Average action potential (AP) waveforms obtained from 30 seconds of

277   pacemaking of the same cells in (C). **(E)** Phase plot of the average AP waveforms in

278   (D). **(F)** Membrane capacitance and **(G)** input resistance of SNc (blue squares) and

279   PPN (red circles) neurons measured using a -5 mV step from the holding potential of

280   -70 mV. **(H)** Spontaneous firing frequency (no current injected) of SNc and PPN

281   neurons. **(I)** The firing regularity, represented by the coefficient of variation (CV) of

282   the interspike interval (ISI), **(J)** interspike membrane potential (mV), **(K)** AP threshold

283   potential, **(L)** AP spike height, **(M)** AP half-width, and **(N)** AP trough (the lowest Vm

284   during afterhyperpolarization) of spontaneously firing SNc and PPN neurons.

285

Sodium channel blockage decreases tonic calcium in PPN cholinergic neurons

In SNc dopaminergic neurons, AP backpropagation into the dendrites can sensitively regulate Ca^{2+} entry (Hage and Khaliq, 2015; Wilson and Callaway, 2000) and neurotransmitter release (Beckstead et al., 2004; Gantz et al., 2013; Rice et al., 1997) in a frequency-dependent manner. Two major sources of Ca^{2+} account for the Ca^{2+} influx during firing activity: AP-evoked Ca^{2+} and Ca^{2+} entry at subthreshold voltages. Previous work has shown that subthreshold depolarization contributes greatly to dendritic Ca^{2+} levels even in the absence of firing in SNc dopaminergic neurons (Chan et al., 2007; Guzman et al., 2009; Hage and Khaliq, 2015). To test which mechanism mediates activity-associated Ca^{2+} increase in PPN cholinergic neurons and to directly compare the results with SNc dopaminergic neurons, we filled the patch pipette with the green Ca^{2+}-sensitive dye Fluo-5F and imaged the soma and dendrites of PPN or SNc neurons during tonic and phasic firing. Linescans were taken at three sites on one cell (Fig. 2A): soma, proximal dendrite ($\leq$50 μm), and distal dendrites (>50 μm). Ca^{2+} signals were calculated by dividing the changes in green fluorescence by red fluorescence and normalized to saturated Ca^{2+} conditions (presented as G/Gs, Fig. 2B). During tonic firing, a Ca^{2+} transient closely correlating to each peak of somatic AP ("pacemaking Ca^{2+}") could be observed in the soma of 3.8% (1 out of 26), in the proximal dendrites of 46% (12 out of 26), and in the distal dendrites of 42% (11 out of 26) of the imaged PPN neurons. The peaks of pacemaking Ca^{2+} were especially prominent in the dendrites of slow-firing cells (<3 Hz), but often undefinable in the soma or in faster-firing cells. To observe phasic Ca^{2+} entry, a 200-pA current step was applied to evoke burst-like firing and a robust Ca^{2+} transient during the linescan imaging (Fig. 1C).

To evaluate the relationship between somatodendritic Ca^{2+} and AP frequency in PPN neurons, we plotted the basal Ca^{2+} levels against the simultaneous tonic firing frequency of PPN neurons alongside the SNc neuron data for comparison. The data from one cell type at each cellular compartment were fitted to linear regression. Interestingly, basal Ca^{2+} levels in PPN neurons were highly correlated with firing rates in all somatodendritic compartments, having a statistically significant correlation coefficient (r) value of 0.8759 at the soma (n = 9, p = 0.0020; Fig. 2D), 0.8875 at the

proximal dendrites (n = 9, p = 0.0014; Fig. 2E), and 0.8318 at the distal dendrites (n = 9, p = 0.0054; Fig 2F). The relationship between basal Ca^{2+} levels and firing rates showed less correlation and did not reach statistical significance in all somatodendritic compartments of SNc neurons. The r value at the SNc soma was 0.4690 (n = 8, p = 0.2411), 0.2191 at the proximal dendrite (n = 8, p = 0.6022), and 0.5731 at the distal dendrite (n = 7, p = 0.1787). The lower r values in the SNc are consistent with previous findings that dendritic Ca^{2+} in SNc dopaminergic neurons are mostly induced by subthreshold depolarization and therefore not necessarily correlated with AP firing, whereas the high r values in the PPN suggest most of the Ca^{2+} is AP-evoked and frequency-dependent.

We tested the hypothesis that dendritic Ca^{2+} in the PPN is AP-dependent by silencing the sodium channel-mediated spikes with TTX. After bath application of TTX (500 nM), AP spiking in PPN neurons was effectively silenced, revealing a stable and rather depolarized Vm (Fig. 2G). This inhibition of tonic firing significantly decreased the basal Ca^{2+} levels in the soma from 0.165 ± 0.012 to 0.127 ± 0.012 G/Gs (n = 10, Wilcoxon signed-rank test, p = 0.0020; Fig. 2H), proximal dendrites from 0.168 ± 0.014 to 0.127 ± 0.009 G/Gs (n = 10, Wilcoxon signed-rank test, p = 0.0059; Fig. 2I), and distal dendrites from 0.182 ± 0.016 to 0.120 ± 0.009 G/Gs (n = 7, Wilcoxon signed-rank test, p = 0.0488; Fig. 2J). In contrast, during evoked phasic firing, TTX caused a drop in basal Ca^{2+} levels but the amplitudes of depolarization-induced Ca^{2+} transients (peak − basal Ca^{2+}) were not changed in any somatodendritic compartment (Wilcoxon signed-rank test, phasic Ca^{2+} before vs. after TTX; soma: n = 10, p = 0.5566; proximal dendrite: n = 10, p = 0.6953; distal dendrite: n = 7, p = 0.8125; Fig. 2K-N). These results suggest that, similar to SNc dopaminergic neurons, PPN cholinergic neurons exhibit pacemaking Ca^{2+} that corresponds to somatic APs. AP firing contributes to a significant component of somatodendritic Ca^{2+} during tonic firing in PPN neurons, but the Ca^{2+} entry during phasic depolarization does not require AP firing or the activation of TTX-sensitive sodium channels.
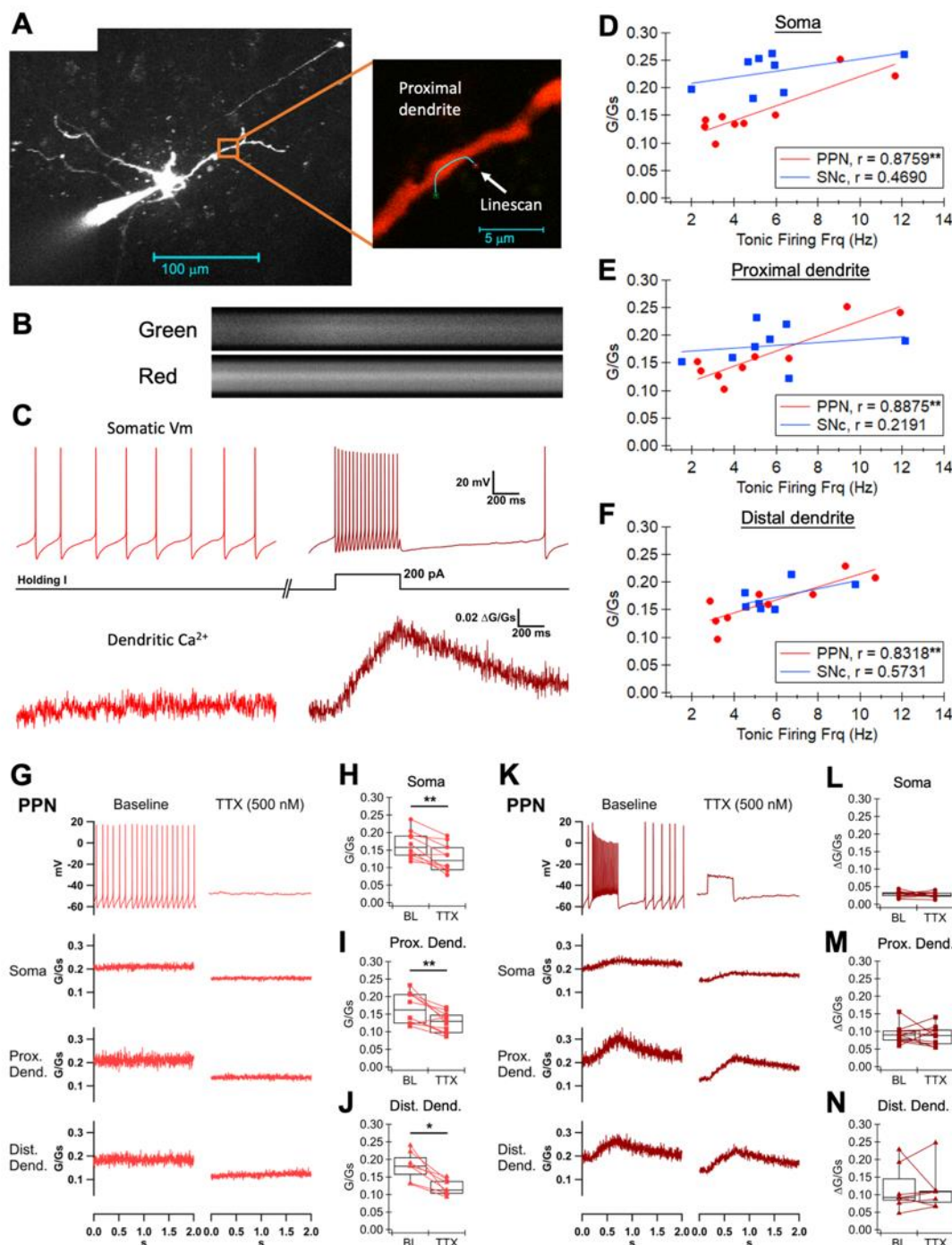
Figure 2. Dendritic calcium recordings in PPN cholinergic neurons with and without sodium channel blockade. (A) Representative image showing the morphology of a PPN cholinergic neuron with a patch pipette filled with Alexa Fluor 594 and Fluo-5F (left) and a zoomed-in image of the area indicated by the orange square showing the site of linescan taken at the proximal dendrite of the neuron (right). **(B)** Linescan fluorescence signals (separated into green and red channels) showing a Ca^{2+} transient during a 200-pA current step measured at the dendrite in (A). **(C)** Time-

358   matched whole-cell somatic Vm recording and dendritic linescan Ca^{2+} signal during 0

359   pA holding current (light red) and a 200-pA current step (dark red), measured at the

360   dendrite in (A). In this representative recording, pacemaking Ca^{2+} was observed in

361   the basal condition (0 pA). **(D)** The basal Ca^{2+} level measured at the soma, **(E)**

362   proximal dendrite ($\leq$50 μm), and **(F)** distal dendrite (>50 μm) plotted against the

363   tonic firing frequency measured at the soma of PPN (red circles) and SNc (blue

364   squares) neurons. The data from one cell type at each location were fitted to linear

365   regression. The corresponding Pearson correlation coefficients (r) and statistical

366   significance are shown. **(G)** Representative time-matched recordings of somatic Vm

367   and Ca^{2+} signals measured at the soma, proximal dendrite, and distal dendrite of a

368   PPN cholinergic neuron during 0 pA holding current at the baseline and after bath

369   treatment of tetrodotoxin (TTX, 500 nM). **(H)** Summary box plot of the basal Ca^{2+}

370   levels measured at the soma, **(I)** proximal dendrite, and **(J)** distal dendrite at the

371   baseline (BL) and after TTX treatment. **(K)** Representative time-matched recordings

372   of somatic Vm and Ca^{2+} signals measured at the soma, proximal dendrite, and distal

373   dendrite of a PPN cholinergic neuron during 200-pA current step at the baseline and

374   after bath treatment of TTX. **(L)** Summary box plot of the phasic Ca^{2+} amplitudes

375   (peak $-$ basal Ca^{2+}) measured at the soma, **(M)** proximal dendrite, and **(N)** distal

376   dendrite at the baseline and after TTX treatment.

377

L-type calcium channel blockage has minimal effects on action potential kinetics in

PPN cholinergic neurons

Because TTX inhibition of AP firing in PPN neurons caused a significant reduction in basal Ca^{2+} levels, we hypothesized that most of the tonic activity-associated Ca^{2+} influx occurs during the AP. This is in contrast to SNc neurons, in which the low-threshold L-type Ca^{2+} channel Cav1.3 activates at subthreshold voltages and mediates most of the Ca^{2+} influx during pacemaking (Chan et al., 2007; Philippart et al., 2016; Puopolo et al., 2007). To further investigate the mechanisms mediating activity-associated Ca^{2+} entry in PPN neurons, and whether L-type Ca^{2+} channels play a similar role in the regulation of AP kinetics in SNc and PPN neurons, we treated the two cell types with the L-type Ca^{2+} channel blocker nifedipine and compared the changes in their AP properties.

Consistent with pacemaking Ca^{2+} in SNc neurons depending on L-type Ca^{2+} channels, nifedipine (10 μM) bath treatment caused a modest but significant reduction in tonic firing rate from 5.74 ± 0.94 to 4.60 ± 0.74 Hz in SNc neurons (n = 8, Wilcoxon signed-rank test, p = 0.039; Fig. 3C). Accompanying the decrease in firing rate, there was a widening of the AP spike, from 1.70 ± 0.08 to 2.09 ± 0.16 ms in the half-width (n = 8, Wilcoxon signed-rank test, p = 0.023; Fig. 3D); this slowing of AP kinetics is clearly visible in the representative AP waveform (Fig. 3A) and phase plot (Fig. 3B). However, there were no significant changes in the interspike Vm (n = 8, Wilcoxon signed-rank test, p = 0.2500; Fig. 3E) and the depth of afterhyperpolarization trough (n = 8, Wilcoxon signed-rank test, p = 0.148; Fig. 3F). The firing regularity (n = 8, Wilcoxon signed-rank test, p = 0.2500), AP threshold (n = 8, Wilcoxon signed-rank test, p = 0.7422), and spike height (n = 8, Wilcoxon signed-rank test, p = 0.1094) were also not affected by the nifedipine treatment (Supplementary Fig. S1).

However, unlike the SNc neurons, nifedipine did not affect the tonic firing frequency (n = 9, Wilcoxon signed-rank test, p = 1.000; Fig. 3I) or AP half-width (n = 9, Wilcoxon signed-rank test, p = 0.8203; Fig. 3J) of PPN neurons. As shown by the representative AP waveform (Fig. 3G) and phase plot (Fig. 3H), there were minimal changes to the overall AP shape, except a mild but significant depolarization of the interspike Vm

411   from -53.84 ± 1.46 to -52.38 ± 1.50 mV (n = 9, Wilcoxon signed-rank test, p = 0.0195;

412   Fig. 3K) and reduction of afterhyperpolarization trough from -62.69 ± 1.77 to -60.23 ±

413   1.75 mV (n = 9, Wilcoxon signed-rank test, p = 0.0004; Fig. 3L). The firing regularity (n

414   = 9, Wilcoxon signed-rank test, p = 0.0742), AP threshold (n = 9, Wilcoxon signed-rank

415   test, p = 0.2031), and spike height (n = 9, Wilcoxon signed-rank test, p = 0.0547) were

416   unaffected by the nifedipine treatment (Supplementary Fig. S1). These results show

417   that the effects of L-type Ca^{2+} channel blockage are distinct in those two cell types:

418   nifedipine slows the kinetics of the AP spike in SNc neurons, whereas in the PPN

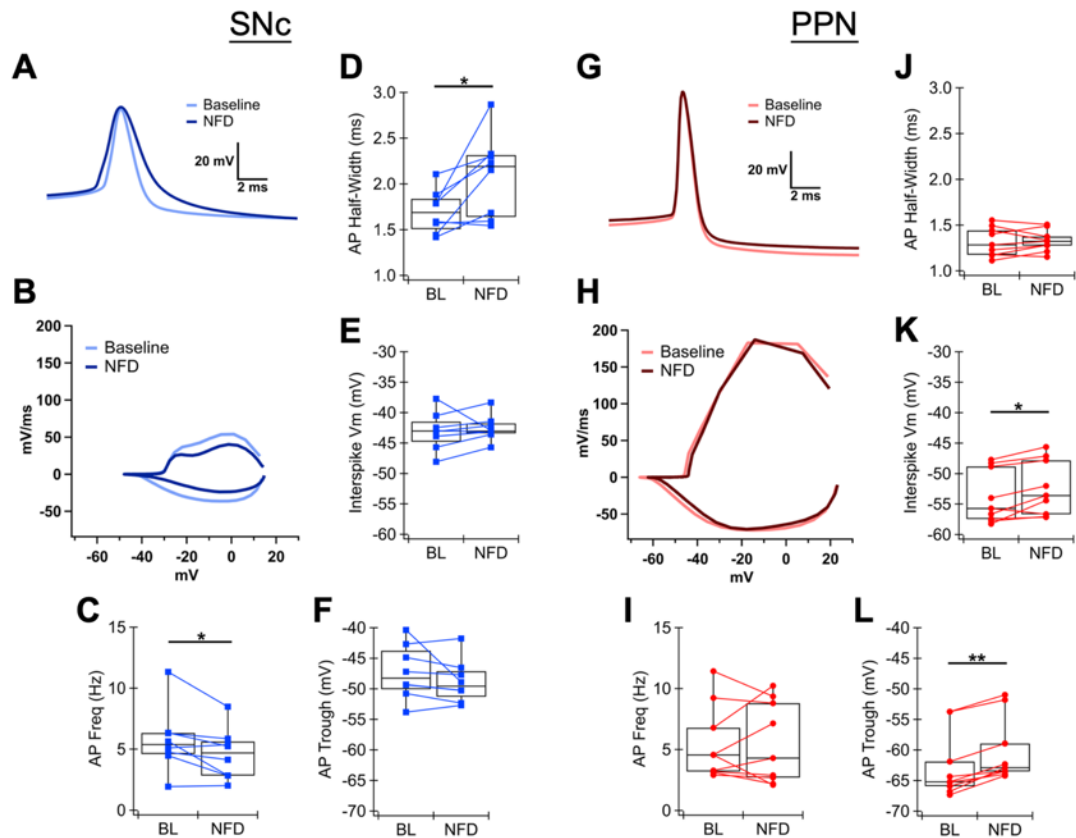419   neurons, nifedipine depolarizes the interspike Vm.

420

Figure 3. L-type calcium channel regulation of action potential shape in PPN and SNc neurons. (A) Average AP waveform of a SNc dopaminergic neuron obtained from 30-s of tonic firing at the baseline (BL, light blue) and after bath treatment of nifedipine (NFD, 10 μM; dark blue). **(B)** Phase plot of the average AP waveforms in (A). **(C)** Tonic firing frequency, **(D)** AP half-width, **(E)** interspike Vm, and **(F)** afterhyperpolarization trough of SNc neurons at the baseline and after nifedipine treatment. **(G)** Average AP waveform of a PPN cholinergic neuron obtained from 30-s of tonic firing at the baseline (light red) and after bath treatment of nifedipine (dark red). **(H)** Phase plot of the average AP waveforms in (G). **(I)** Tonic firing frequency, **(J)** AP half-width, **(K)** interspike Vm, and **(L)** afterhyperpolarization trough of SNc neurons at the baseline and after nifedipine treatment.

18

L-type calcium channel blockage does not reduce tonic calcium in PPN cholinergic neurons

We established that blockage of L-type Ca^{2+} channels affected the kinetics of tonic firing to a lesser extent in PPN neurons than in SNc neurons. This suggests that the pacemaking of PPN neurons may be less reliant on L-type Ca^{2+} conductance, and L-type Ca^{2+} current likely accounts for a smaller portion of depolarization-induced Ca^{2+} influx in PPN neurons. To determine whether L-type Ca^{2+} channels play a significant role in pacemaking Ca^{2+} in PPN neurons, we took two-photon dendritic linescan imaging of tonically firing PPN neurons before and after nifedipine treatment, and compared the change in tonic Ca^{2+} levels to that of SNc neurons.

PPN neurons exhibited heterogeneous responses to nifedipine bath treatment. In one PPN neuron, whose tonic firing rate (from 3.67 to 3.81 Hz) and firing regularity (CV of ISI from 43.23 to 45.07%) were almost identical before and after nifedipine, the basal Ca^{2+} level in the proximal dendrite also remained constant (from 0.127 to 0.128 G/Gs; Fig. 4A). The dendritic Ca^{2+} oscillated with AP spiking, but the peaks were less defined and only slightly reduced in nifedipine. In another PPN neuron, the tonic firing became much slower (from 4.69 to 1.66 Hz) and more irregular (CV of ISI from 8.30 to 25.30%) after nifedipine treatment, and the basal Ca^{2+} level in the proximal dendrite was likewise reduced (from 0.141 to 0.120 G/Gs; Fig. 4B). This cell exhibited clear pacemaking Ca^{2+}, having well-defined peaks that neatly correlated with AP spiking and were greatly reduced by nifedipine treatment. Therefore, we observed that some PPN cholinergic neurons appear sensitive to nifedipine, while others are unresponsive. When the results were averaged across all PPN cells, there were no significant changes in the basal Ca^{2+} levels after nifedipine in any somatodendritic compartment during tonic firing (Wilcoxon signed-rank test, tonic Ca^{2+} before vs. after nifedipine; soma: n = 10, p = 0.1934; proximal dendrite: n = 10, p = 0.1309; distal dendrite: n = 10, p = 0.1309; Fig. 4C-F). The unaltered tonic Ca^{2+} levels correspond to the lack of change in the averaged firing frequency in PPN neurons after L-type Ca^{2+} channel blockage.

Because there is a well-defined role for low-threshold L-type Ca^{2+} channels (Cav1.3)

468   in SNc dopaminergic neuron tonic Ca^{2+} levels (Chan et al., 2007; Guzman et al., 2009;

469   Hage and Khaliq, 2015; Puopolo et al., 2007), we ran the same experiments on SNc

470   neurons. In contrast to the lack of effect in PPN neurons, nifedipine exerted a

471   significant and consistent effect on the tonic Ca^{2+} levels in SNc neurons (Fig. 4G).

472   Accompanying the slowing of tonic firing frequency and AP kinetics, the basal Ca^{2+}

473   levels in the soma (from 0.229 ± 0.012 to 0.187 ± 0.011 G/Gs, n = 8, Wilcoxon signed-

474   rank test, p = 0.0078; Fig. 4H), proximal dendrites (from 0.181 ± 0.013 to 0.146 ±

475   0.011 G/Gs, n = 8, Wilcoxon signed-rank test, p = 0.0078; Fig. 4I), and distal dendrites

476   (from 0.173 ± 0.009 to 0.119 ± 0.011 G/Gs, n = 7, Wilcoxon signed-rank test, p =

477   0.0156; Fig. 4J) of SNc neurons were all significantly decreased by nifedipine. This

478   trend was strong and consistent across cells, as all 8 SNc neurons recorded showed

479   decreases in tonic Ca^{2+} in all somatodendritic compartments after nifedipine

480   treatment. Therefore, in the same recording conditions, L-type Ca^{2+} channel blockage

481   reduces tonic dendritic Ca^{2+} in SNc dopaminergic neurons, but not in PPN cholinergic
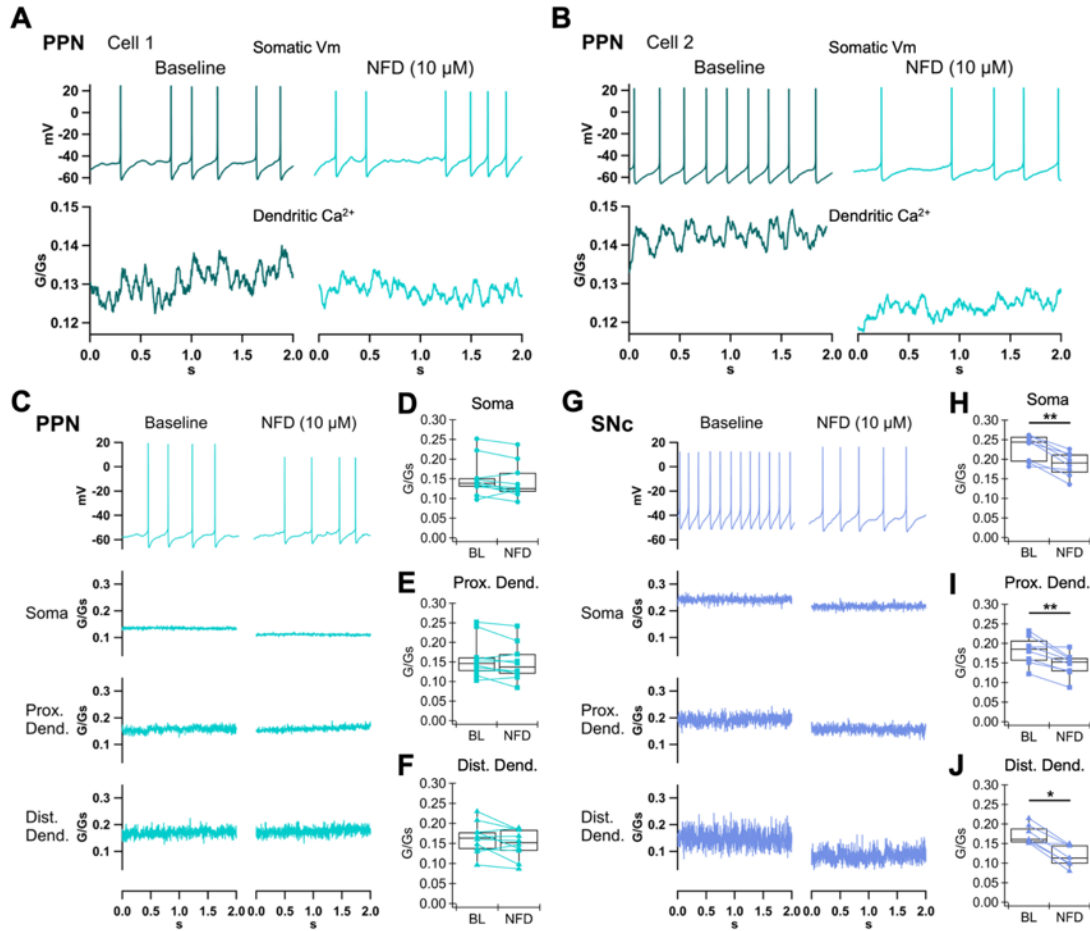
482   neurons.

483

Figure 4. Contribution of L-type channels to PPN and SNc tonic calcium. (A) Example
PPN cholinergic neuron whose tonic firing rate and basal Ca^{2+} level measured at the
proximal dendrite did not change after nifedipine (NFD, 10 µM) bath treatment. **(B)**
Example PPN cholinergic neuron whose tonic firing rate and basal Ca^{2+} level
measured at the proximal dendrite both decreased after nifedipine treatment. The
Ca^{2+} traces in (A) and (B) were smoothed using the boxcar method with a factor of 20
points. Pacemaking Ca^{2+} that correlated with AP spiking could be seen in the baseline
condition. **(C)** Representative time-matched recordings of somatic Vm and Ca^{2+}
signals measured at the soma, proximal dendrite, and distal dendrite of a PPN
cholinergic neuron during 0 pA holding current at the baseline and after nifedipine
treatment. **(D)** Summary box plot of the basal Ca^{2+} levels measured at the soma, **(E)**
proximal dendrite, and **(F)** distal dendrite of PPN cholinergic neurons at the baseline
(BL) and after nifedipine treatment. **(G)** Representative time-matched recordings of
somatic Vm and Ca^{2+} signals measured at the soma, proximal dendrite, and distal
dendrite of a SNc dopaminergic neuron during 0 pA holding current at the baseline
and after nifedipine treatment. **(H)** Summary box plot of the basal Ca^{2+} levels
measured at the soma, **(I)** proximal dendrite, and **(J)** distal dendrite of SNc
dopaminergic neurons at the baseline and after nifedipine treatment.

L-type calcium channel blockage decreases phasic calcium in PPN cholinergic neurons

To determine whether L-type Ca^{2+} channels play a significant role in depolarization-induced Ca^{2+} entry during phasic firing in PPN neurons, we applied a 200-pA current step to elicit a burst of fast phasic firing and elevation of somatodendritic Ca^{2+}. Nifedipine significantly decreased the amplitudes of phasic firing-induced Ca^{2+} entry in all somatodendritic compartments in the PPN neurons (Fig. 5A), from 0.033 ± 0.003 to 0.028 ± 0.003 $\Delta G/Gs$ in the soma (n = 10, Wilcoxon signed-rank test, p = 0.0195; Fig. 5B), 0.104 ± 0.011 to 0.081 ± 0.012 $\Delta G/Gs$ in the proximal dendrites (n = 10, Wilcoxon signed-rank test, p = 0.0137; Fig. 5C), and 0.109 ± 0.010 to 0.072 ± 0.008 $\Delta G/Gs$ in the distal dendrites (n = 10, Wilcoxon signed-rank test, p = 0.0020; Fig. 5D). DMSO (0.05%) alone had no effects on phasic Ca^{2+} in the soma (n = 6, Wilcoxon signed-rank test, p = 0.1563) and proximal dendrites (n = 6, Wilcoxon signed-rank test, p = 0.5625) of PPN neurons, while there was a statistically significant decrease of phasic Ca^{2+} amplitudes in the distal dendrite (n = 6, Wilcoxon signed-rank test, p = 0.0313; Supplementary Fig. S2). This indicates that the phasic Ca^{2+} signal in the distal dendrites undergoes rundown over time. The efficacy of nifedipine in reducing phasic Ca^{2+} in the soma and proximal dendrites suggests that fast burst-like firing in PPN neurons can reliably activate L-type Ca^{2+} channels, and that these channels are likely to be the high-threshold (Cav1.2) subtype.

When the same protocol was performed in SNc neurons (Fig. 5E), we found that nifedipine significantly reduced the amplitude of phasic Ca^{2+} in the soma, from 0.035 ± 0.005 to 0.023 ± 0.001 $\Delta G/Gs$ (n = 8, Wilcoxon signed-rank test, p = 0.0156; Fig. 5F). Phasic Ca^{2+} in the proximal and distal dendrites showed trends of decrease in nifedipine, but the effects did not reach statistical significance (proximal dendrite: n = 8, Wilcoxon signed-rank test, p = 0.0547; distal dendrites: n = 7, Wilcoxon signed-rank test, p = 0.0781; Fig. 5G-H). This result supports the idea that Cav1.2 is more weakly expressed than the low-threshold Cav1.3 L-type channels in SNc dopaminergic neurons (Chan et al., 2007; Dufour et al., 2014; Philippart et al., 2016). Together, our results suggest that L-type Ca^{2+} channels play opposing roles in tonic vs. phasic Ca^{2+} entry in PPN and SNc neurons: while L-type Ca^{2+} channels contribute significantly to tonic Ca^{2+} but less to phasic Ca^{2+} in SNc neurons, the same family of channels account for a significant amount of phasic Ca^{2+} but not tonic Ca^{2+} in PPN neurons.
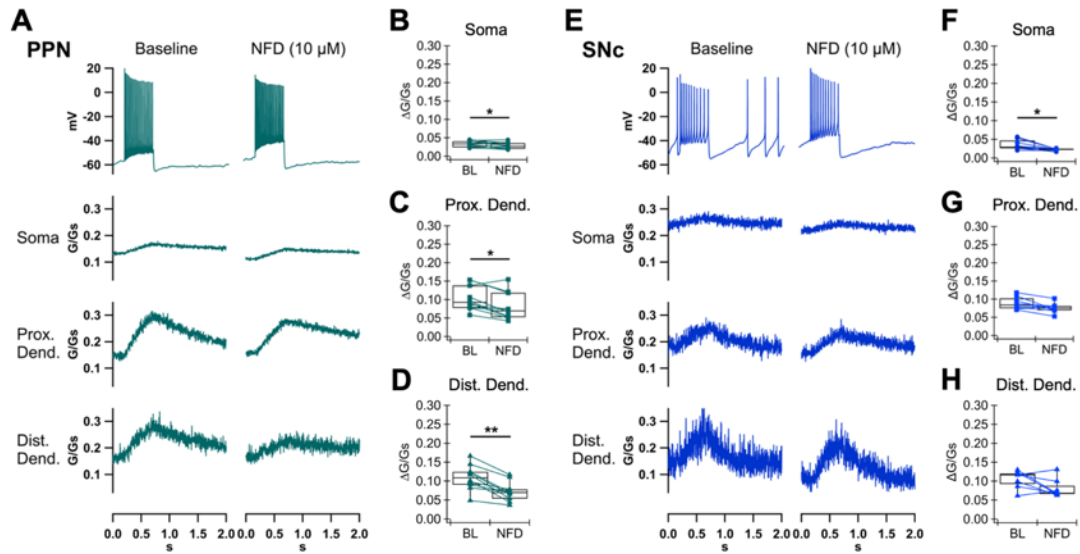
Figure 5. Contribution of L-type channels to PPN and SNc phasic calcium. (A)
Representative time-matched recordings of somatic Vm and Ca^{2+} signals measured at
the soma, proximal dendrite, and distal dendrite of a PPN cholinergic neuron during
200-pA current step at the baseline and after bath treatment of nifedipine (NFD). **(B)**
Summary box plot of the phasic Ca^{2+} amplitudes (peak − basal Ca^{2+}) measured at the
soma, **(C)** proximal dendrite, and **(D)** distal dendrite of PPN cholinergic neurons at
the baseline (BL) and after nifedipine treatment. **(E)** Representative time-matched
recordings of somatic Vm and Ca^{2+} signals measured at the soma, proximal dendrite,
and distal dendrite of a SNc dopaminergic neuron during 200-pA current step at the
baseline and after bath treatment of nifedipine. **(F)** Summary box plot of the phasic
Ca^{2+} amplitudes measured at the soma, **(G)** proximal dendrite, and **(H)** distal dendrite
of SNc dopaminergic neurons at the baseline and after nifedipine treatment.

L-type calcium channels contribute to tonic calcium levels throughout the dendrites in SNc but not PPN neurons

Previous studies showed that depolarization-induced Ca^{2+} signals, which could be evoked by AP backpropagation, travel along the dendrites of SNc dopaminergic neurons and decay very little with distance (Hage and Khaliq, 2015). This is due to strong electronic coupling of the soma and the dendrites, as well as the presence of Ca^{2+} channels active at subthreshold potentials. In this study, we found that PPN neurons have higher input resistance than SNc neurons, suggesting even tighter electronic coupling throughout the cell. However, PPN neurons appear to express only high-threshold L-type Ca^{2+} channels, which would require significant depolarization invading into the dendrites to activate. To determine the amounts of L-type Ca^{2+} channel-mediated Ca^{2+} influx throughout the dendrites, we evaluated the nifedipine-dependent reduction in tonic Ca^{2+} signals between SNc and PPN neurons across distances from the soma.

To directly compare the role of L-type Ca^{2+} channels in SNc and PPN dendrites, we grouped the Ca^{2+} data into three compartments: soma, proximal dendrite, and distal dendrite (Fig. 6G). In the box plots, the $\Delta G/Gs$ value is calculated from subtracting the Ca^{2+} level after nifedipine treatment from the control Ca^{2+} level (Ca^{2+} before nifedipine − after nifedipine); therefore, a positive $\Delta G/Gs$ indicates a decrease of Ca^{2+} level by nifedipine while a negative $\Delta G/Gs$ indicates an increase. The reduction of basal Ca^{2+} during tonic firing due to nifedipine was significantly larger in the soma of SNc neurons than in the soma of PPN neurons (SNc soma: 0.042 ± 0.006 $\Delta G/Gs$, n = 8; PPN soma: 0.009 ± 0.005 $\Delta G/Gs$, n = 10; Mann-Whitney-Wilcoxon test, p = 0.0021; Fig. 6A). Similarly, nifedipine caused a significantly larger reduction of tonic Ca^{2+} in the proximal and distal dendrites of SNc neurons, compared to the proximal and distal dendrites of PPN neurons, respectively (SNc proximal dendrites: 0.036 ± 0.008 $\Delta G/Gs$, n = 8; PPN proximal dendrites: 0.010 ± 0.005 $\Delta G/Gs$, n = 10; Mann-Whitney-Wilcoxon test, p = 0.0117; Fig. 6B. SNc distal dendrites: 0.054 ± 0.009 $\Delta G/Gs$, n = 7; PPN distal dendrites: 0.015 ± 0.008 $\Delta G/Gs$, n = 10; Mann-Whitney-Wilcoxon test, p = 0.0046; Fig. 6C). By contrast, when the reduction of phasic firing-evoked Ca^{2+} due to nifedipine was compared, there was no significant difference between SNc and PPN

587   neurons at the soma (SNc: n = 8; PPN: n = 10; Mann-Whitney-Wilcoxon test, p =

588   0.3599; Fig. 6D), proximal dendrites (SNc: n = 8; PPN: n = 10; Mann-Whitney-

589   Wilcoxon test, p = 0.2031; Fig. 6E), or distal dendrites (SNc: n = 7; PPN: n = 10; Mann-

590   Whitney-Wilcoxon test, p = 0.4747; Fig. 6F). Thus, our results show that nifedipine

591   has consistently larger effects on tonic Ca^{2+} in SNc neurons regardless of distances

592   from the soma. This suggests that SNc neurons have larger L-type Ca^{2+} channel-

593   mediated tonic influx throughout the dendrites compared to PPN neurons.

594

595   To more precisely evaluate the role of L-type Ca^{2+} channels across the extent of the

596   dendritic arbor, we plotted the Ca^{2+} reduction due to nifedipine by the distances

597   from the soma. We found that the tonic Ca^{2+} reduction due to nifedipine was

598   consistently larger in SNc neurons compared to PPN neurons throughout the extent

599   of the dendritic arbor. This is demonstrated by the SNc trendline having a much

600   larger y-intercept value of 0.038 ± 0.001 ΔG/Gs than that of the PPN trendline, 0.006

601   ± 0.001 ΔG/Gs, while the two trendlines have similar slopes: $8.86 \times 10^{-5} \pm 1.06 \times 10^{-5}$

602   (ΔG/Gs)/μm for SNc and $6.65 \times 10^{-5} \pm 0.88 \times 10^{-5}$ (ΔG/Gs)/μm for PPN (Fig. 6H).

603   These data indicate that L-type Ca^{2+}channels (likely the low-threshold Cav1.3

604   subtype) contribute to tonic pacemaking Ca^{2+} influx throughout the somatodendritic

605   extent of SNc neurons, but do not contribute to tonic Ca^{2+} influx in any compartment

606   of the PPN neurons.

607

608   Evaluating the nifedipine effect on phasic Ca^{2+}, we found no difference in SNc and

609   PPN neurons at locations closer to the soma, shown by the SNc and PPN trendlines

610   crossing near the y-intercepts (SNc y-intercept: 0.014 ± 0.001 ΔG/Gs; PPN y-

611   intercept: 0.013 ± 0.001 ΔG/Gs; Fig. 6I). In the distal dendrites, the PPN trendline has

612   a steeper slope value of $1.38 \times 10^{-4} \pm 0.09 \times 10^{-4}$ (ΔG/Gs)/μm, which was almost 10

613   times of the slope value of the SNc trendline, $2.32 \times 10^{-5} \pm 1.05 \times 10^{-5}$ (ΔG/Gs)/μm.

614   These results indicate that L-type Ca^{2+} channels (likely the high-threshold Cav1.2

615   subtype) contribute to phasic Ca^{2+} influx more substantially in the distal dendrites of

616   PPN neurons, whereas these high-threshold channels make minimal but uniform

617   contributions to phasic Ca^{2+} influx across SNc somatodendritic

618   compartments.Together, our findings show that L-type Ca^{2+} channels contribute to

619   phasic, but not tonic Ca^{2+} levels in PPN cholinergic neurons.

Figure 6. Contribution of L-type channels throughout the dendrites of PPN and SNc neurons. (A) The difference in the basal Ca^{2+} levels (during tonic firing at 0 pA holding current) before and after bath treatment of nifedipine (Ca^{2+} before NFD − after NFD) in SNc dopaminergic (light blue squares) and PPN cholinergic (light red circles) neurons, measured at the soma, **(B)** proximal dendrite, and **(C)** distal dendrite. **(D)**

The difference in the amplitudes of phasic Ca^{2+} evoked by a 200-pA current step before and after bath treatment of nifedipine in SNc dopaminergic (dark blue squares) and PPN cholinergic (dark red circles) neurons, measured at the soma, **(E)** proximal dendrite, and **(F)** distal dendrite. **(G)** Example linescan sites, indicated by colored bars, taken at the soma (orange), proximal dendrite (yellow), and distal dendrite (green) of a PPN cholinergic neuron. **(H)** The difference in the basal Ca^{2+} levels before and after nifedipine treatment in SNc dopaminergic (light blue squares) and PPN cholinergic (light red circles) neurons plotted against distance from the soma of the linescan site. **(I)** The difference in the amplitudes of phasic Ca^{2+} before and after nifedipine treatment in SNc dopaminergic (dark blue squares) and PPN cholinergic (dark red circles) neurons plotted against distance from the soma of the linescan site. The data from each cell type were fitted to linear regression.

640   Discussion

641

642   Our study finds that PPN cholinergic neurons display similar spontaneous firing

643   properties and pacemaking-induced Ca^{2+} oscillations as SNc dopaminergic neurons,

644   but that, unlike SNc neurons, tonic Ca^{2+} entry in PPN neurons is not mediated by L-

645   type Ca^{2+} conductance. Since somatodendritic tonic Ca^{2+} levels in PPN neurons are

646   strongly decreased by TTX-induced sodium channel blockage, but not by nifedipine-

647   induced L-type Ca^{2+} channel blockage, our data indicate that most of the tonic Ca^{2+} in

648   PPN neurons is AP-evoked. In contrast, burst-like phasic firing-induced Ca^{2+} transients

649   in PPN neurons were significantly suppressed by nifedipine, supporting the idea that

650   PPN neurons selectively express high-threshold L-type Ca^{2+} channels. In addition, we

651   show that L-type channel blockage slowed the kinetics of APs in SNc dopaminergic

652   neurons but had minimal effects on PPN cholinergic neurons, indicating the

653   pacemaking activities of these two midbrain neuronal populations are regulated by

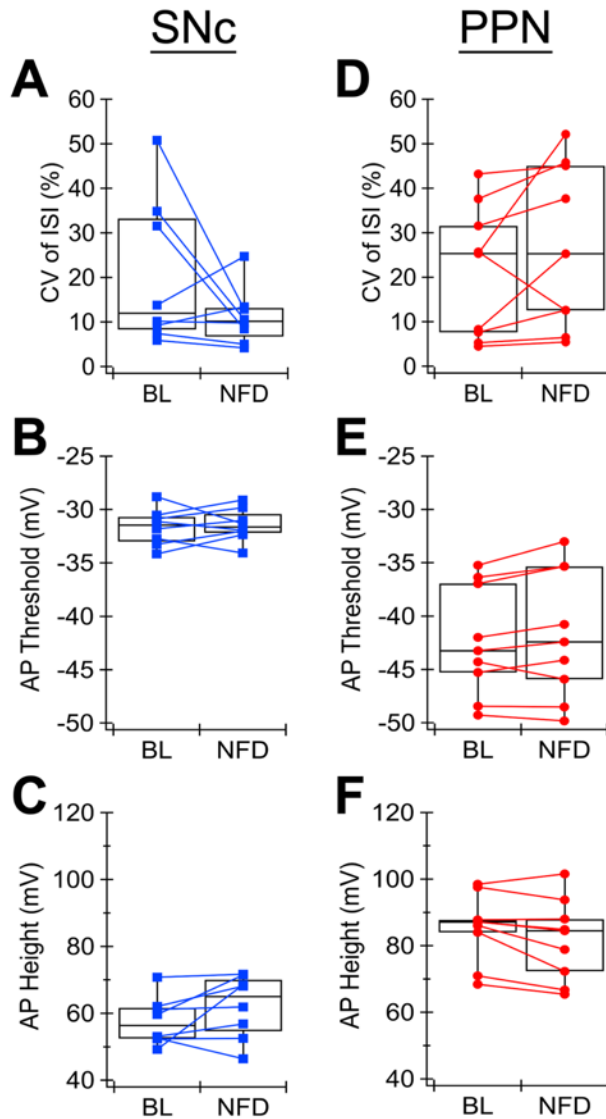654   fundamentally different ionic mechanisms.

655

656   The majority of research investigating cellular mechanisms in Parkinson's disease has

657   been done on SNc dopaminergic neurons, while there is a lack of understanding of

658   the relevant basic physiological properties of PPN cholinergic neurons. Takakusaki &

659   Kitai were the first to report high-threshold somatic Ca^{2+} oscillations mediated by L-

660   and N-type Ca^{2+} channels in the PPN cholinergic neurons of male adolescent rats

661   (Takakusaki and Kitai, 1997). More than a decade later, work from the Garcia-Rill Lab

662   identified N- and P/Q-type Ca^{2+} channels as the ionic mechanisms underlying high-

663   threshold somatic Ca^{2+} oscillations in PPN cholinergic neurons in young rats

664   (Kezunovic et al., 2011), and imaged these high-threshold Ca^{2+} oscillations using

665   ratiometric fluorescence Ca^{2+} sensors (Hyde et al., 2013). Although they showed that

666   a depolarizing current ramp evoked Ca^{2+} transient in the soma as well as the proximal

667   dendrites, suggesting the presence of Ca^{2+} channels throughout the cell, they did not

668   measure Ca^{2+} in distal dendrites. Here, we measured activity-associated Ca^{2+} entry in

669   distal dendrites up to 300 μm away from the soma, and directly compared PPN and

670   SNc neurons in the same experimental design. We found that tonic Ca^{2+} in PPN

671   neurons is depended on sodium channel-mediated spiking, whereas the propagation

672   of phasic Ca^{2+} into the dendrites does not require AP firing. This is consistent with

673   previous findings that the somatic Ca^{2+} transients induced by a depolarizing current

674   ramp were unchanged or even larger in the presence of TTX (Hyde et al., 2013). We

675   also found that nifedipine did not reduce tonic Ca^{2+} but inhibited a significant portion

676   of phasic Ca^{2+} in PPN neurons. In the perspective of past findings, intracellular Ca^{2+}

677   levels of PPN neurons during tonic firing and the nifedipine-insensitive portion of

678 phasic Ca^{2+} likely depend on other high-threshold Ca^{2+} channels, namely the N- and
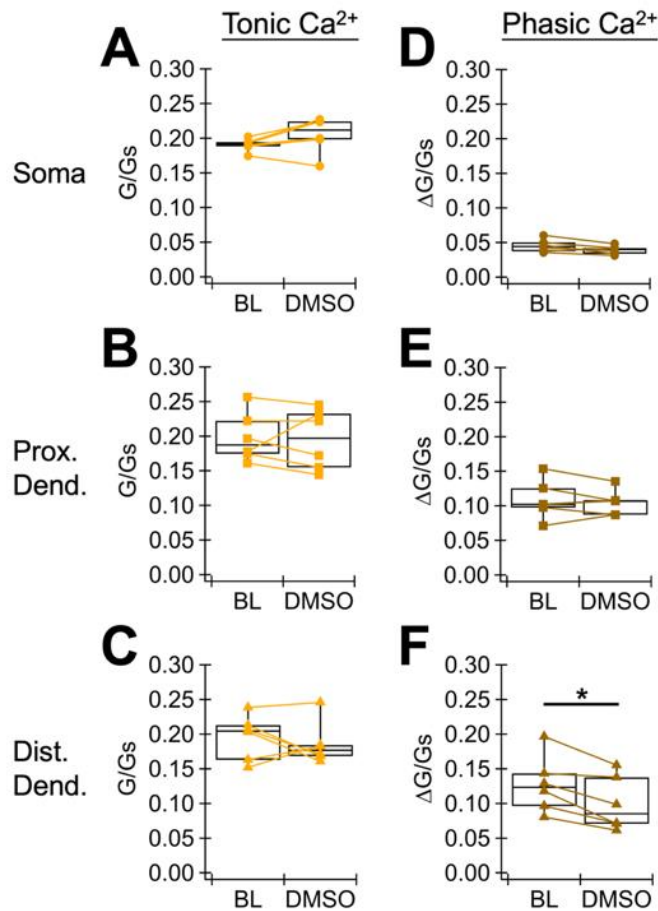
679 P/Q-types.

680

681 In addition to imaging dendritic Ca^{2+}, we investigate the effects of L-type channel

682 blockage on PPN neuron AP kinetics. Our results show that the only significant effect

683 of nifedipine on PPN neuron AP shape was a slight depolarization of the interspike

684 Vm, including the afterhyperpolarization trough. Surprisingly, while nifedipine

685 significantly decreased firing frequency and increased spike width in SNc neurons,

686 there was no change in the interspike Vm. We suggest that these distinct nifedipine

687 effects on the membrane potential could be caused by the interplay of different L-

688 type Ca^{2+} channel subtypes and Ca^{2+}-activated potassium channels. In both PPN and

689 SNc neurons, apamin-sensitive SK channels have been reported to underlie the

690 afterhyperpolarization phase of AP or Ca^{2+} oscillations (de Vrind et al., 2016; Ping and

691 Shepard, 1996; Takakusaki and Kitai, 1997). In PPN neurons, nifedipine could be

692 blocking the high-threshold L-type Ca^{2+} channels activated during the AP spike,

693 leading to less Ca^{2+} activation of SK channels to deepen the afterhyperpolarization

694 trough and interspike Vm. In SNc neurons, the unaltered interspike Vm after

695 nifedipine treatment could be the result of changing multiple conductances that

696 compensate one another's effect. While the low-threshold L-type Ca^{2+} channels are

697 blocked by nifedipine, which would reduce interspike subthreshold depolarization,

698 there is less Ca^{2+} entry to activate SK channels and SK-mediated hyperpolarization.

699 Therefore, our results from studying AP kinetics are consistent with the idea that SNc

700 neurons predominantly express the low-threshold subtypes and PPN neurons the

701 high-threshold subtypes of L-type Ca^{2+} channels.

702

703 Interestingly, we observed heterogeneity within PPN cholinergic neuron responses to

704 nifedipine treatment. While nifedipine did not have a statistically significant effect on

705 the levels of tonic Ca^{2+} in PPN cholinergic neurons as a whole, we found that

706 nifedipine decreased the firing frequencies and tonic Ca^{2+} levels while increasing

707 pacemaking irregularity in almost half of the PPN neurons. The firing frequencies and

708 irregularity in the rest of the PPN neurons were unchanged or increased after

709 nifedipine. This suggests the possibility that a subpopulation of PPN neurons may

710 rely on L-type channels for pacemaking and tonic Ca^{2+}. PPN cholinergic neurons have

711 historically been divided into several subgroups based on their electrophysiological

712 properties and anatomical locations (Baksa et al., 2019; Kang and Kitai, 1990). Future

713 studies are needed to determine whether dendritic Ca^{2+} signaling in PPN neurons

714 differs in specific subpopulations.

715

716   In summary, our study shows that PPN cholinergic neurons do not share the
717   characteristic of having low-threshold L-type Ca^{2+} conductance with SNc
718   dopaminergic neurons, and thus there are likely other factors that underlie the
719   selective vulnerability of cholinergic PPN neurons to degeneration. The lack of
720   subthreshold Ca^{2+} conductance may be related to clinical observations that PPN
721   neurons (~30-60% loss) do not degenerate to the same extent as SNc neurons (~70%
722   loss) in PD, and PPN neurons have a larger between-patient variation in the
723   percentage loss (Giguère et al., 2018). Many other intrinsic factors could also
724   contribute to cellular vulnerability. Those relevant to PPN neurons include
725   spontaneous pacemaking activity, having a large soma and extensive axonal arbor,
726   dysfunctional proteostasis, and mitochondrial oxidative stress. Here we show that
727   PPN neurons exhibit spontaneous firing activity and significant tonic Ca^{2+} entry, even
728   though the main source of this pacemaking Ca^{2+} is not low-threshold L-type Ca^{2+}
729   channels. Our data also show that PPN neurons and SNc neurons have comparable
730   soma size and membrane capacitance, suggesting they likely have similar
731   morphology and bioenergetic burden. Future work is needed to determine whether
732   PPN cholinergic neurons are prone to the same proteostatic and mitochondrial stress
733   as SNc dopaminergic neurons, and whether other Ca^{2+} channel subtypes contribute
734   to the vulnerability of brainstem neurons such as the PPN.
735

Supplementary Figure 1. (A) The firing regularity, represented by the coefficient of variation (CV) of the interspike interval (ISI), **(B)** AP threshold potential, and **(C)** AP spike height of SNc dopaminergic neurons at the baseline (BL) and after bath treatment of nifedipine (NFD, 10 μM). **(D)** The firing regularity, **(E)** AP threshold potential, and **(F)** AP spike height of PPN cholinergic neurons at the baseline and after nifedipine treatment.

745

746

747 **Supplementary Figure 2. (A)** Summary box plot of the basal Ca^{2+} levels (during tonic

748 firing at 0 pA holding current) measured at the soma, **(B)** proximal dendrite, and **(C)**

749 distal dendrite of PPN cholinergic neurons at the baseline (BL) and after bath

750 treatment of DMSO (0.05%). **(D)** Summary box plot of the phasic Ca^{2+} amplitudes

751 (peak − basal Ca^{2+}) evoked by a 200-pA current step measured at the soma, **(E)**

752 proximal dendrite, and **(F)** distal dendrite of PPN cholinergic neurons at the baseline

753 and after DMSO treatment.

754

755   References

756

757   Baksa, B., Kovács, A., Bayasgalan, T., Szentesi, P., Kőszeghy, Á., Szücs, P., Pál, B., 2019.
758   Characterization of functional subgroups among genetically identified
759   cholinergic neurons in the pedunculopontine nucleus. Cell. Mol. Life Sci. 76,
760   2799–2815. https://doi.org/10.1007/s00018-019-03025-4

761   Beckstead, M.J., Grandy, D.K., Wickman, K., Williams, J.T., 2004. Vesicular dopamine
762   release elicits an inhibitory postsynaptic current in midbrain dopamine
763   neurons. Neuron 42, 939–946. https://doi.org/10.1016/j.neuron.2004.05.019

764   Braak, H., Ghebremedhin, E., Rüb, U., Bratzke, H., Del Tredici, K., 2004. Stages in the
765   development of Parkinson's disease-related pathology. Cell Tissue Res 318,
766   121–134. https://doi.org/10.1007/s00441-004-0956-9

767   Chambers, N.E., Coyle, M., Sergio, J., Lanza, K., Saito, C., Topping, B., Clark, S.D.,
768   Bishop, C., 2021. Effects of pedunculopontine nucleus cholinergic lesion on
769   gait and dyskinesia in hemiparkinsonian rats. Eur J Neurosci 53, 2835–2847.
770   https://doi.org/10.1111/ejn.15106

771   Chan, C.S., Guzman, J.N., Ilijic, E., Mercer, J.N., Rick, C., Tkatch, T., Meredith, G.E.,
772   Surmeier, D.J., 2007. "Rejuvenation" protects neurons in mouse models of
773   Parkinson's disease. Nature 447, 1081–1086.
774   https://doi.org/10.1038/nature05865

775   de Vrind, V., Scuvée-Moreau, J., Drion, G., Hmaied, C., Philippart, F., Engel, D., Seutin,
776   V., 2016. Interactions between calcium channels and SK channels in midbrain
777   dopamine neurons and their impact on pacemaker regularity: Contrasting
778   roles of N- and L-type channels. Eur J Pharmacol 788, 274–279.
779   https://doi.org/10.1016/j.ejphar.2016.06.046

780   Drobizhev, M., Makarov, N.S., Tillo, S.E., Hughes, T.E., Rebane, A., 2011. Two-photon
781   absorption properties of fluorescent proteins. Nat Methods 8, 393–399.
782   https://doi.org/10.1038/nmeth.1596

783   Dryanovski, D.I., Guzman, J.N., Xie, Z., Galteri, D.J., Volpicelli-Daley, L.A., Lee, V.M.-Y.,
784   Miller, R.J., Schumacker, P.T., Surmeier, D.J., 2013. Calcium entry and α-
785   synuclein inclusions elevate dendritic mitochondrial oxidant stress in
786   dopaminergic neurons. J Neurosci 33, 10154–10164.
787   https://doi.org/10.1523/JNEUROSCI.5311-12.2013

788   Dufour, M.A., Woodhouse, A., Goaillard, J.-M., 2014. Somatodendritic ion channel
789   expression in substantia nigra pars compacta dopaminergic neurons across
790   postnatal development. J Neurosci Res 92, 981–999.
791   https://doi.org/10.1002/jnr.23382

792   Evans, R.C., Zhu, M., Khaliq, Z.M., 2017. Dopamine Inhibition Differentially Controls

793   Excitability of Substantia Nigra Dopamine Neuron Subpopulations through T-
794   Type Calcium Channels. J Neurosci 37, 3704–3720.
795   https://doi.org/10.1523/JNEUROSCI.0117-17.2017

796 Gantz, S.C., Bunzow, J.R., Williams, J.T., 2013. Spontaneous inhibitory synaptic
797   currents mediated by a G protein-coupled receptor. Neuron 78, 807–812.
798   https://doi.org/10.1016/j.neuron.2013.04.013

799 Giguère, N., Burke Nanni, S., Trudeau, L.-E., 2018. On Cell Loss and Selective
800   Vulnerability of Neuronal Populations in Parkinson's Disease. Front Neurol 9,
801   455. https://doi.org/10.3389/fneur.2018.00455

802 Gonzalez-Rodriguez, P., Zampese, E., Surmeier, D.J., 2020. Selective neuronal
803   vulnerability in Parkinson's disease. Prog Brain Res 252, 61–89.
804   https://doi.org/10.1016/bs.pbr.2020.02.005

805 Grabli, D., Karachi, C., Folgoas, E., Monfort, M., Tande, D., Clark, S., Civelli, O., Hirsch,
806   E.C., François, C., 2013. Gait disorders in parkinsonian monkeys with
807   pedunculopontine nucleus lesions: a tale of two systems. J Neurosci 33,
808   11986–11993. https://doi.org/10.1523/JNEUROSCI.1568-13.2013

809 Grace, A.A., Onn, S.P., 1989. Morphology and electrophysiological properties of
810   immunocytochemically identified rat dopamine neurons recorded in vitro. J
811   Neurosci 9, 3463–3481. https://doi.org/10.1523/JNEUROSCI.09-10-
812   03463.1989

813 Guzman, J.N., Sánchez-Padilla, J., Chan, C.S., Surmeier, D.J., 2009. Robust pacemaking
814   in substantia nigra dopaminergic neurons. J Neurosci 29, 11011–11019.
815   https://doi.org/10.1523/JNEUROSCI.2519-09.2009

816 Guzman, J.N., Sanchez-Padilla, J., Wokosin, D., Kondapalli, J., Ilijic, E., Schumacker,
817   P.T., Surmeier, D.J., 2010. Oxidant stress evoked by pacemaking in
818   dopaminergic neurons is attenuated by DJ-1. Nature 468, 696–700.
819   https://doi.org/10.1038/nature09536

820 Hage, T.A., Khaliq, Z.M., 2015. Tonic firing rate controls dendritic Ca2+ signaling and
821   synaptic gain in substantia nigra dopamine neurons. J Neurosci 35, 5823–
822   5836. https://doi.org/10.1523/JNEUROSCI.3904-14.2015

823 Hyde, J., Kezunovic, N., Urbano, F.J., Garcia-Rill, E., 2013. Spatiotemporal properties
824   of high-speed calcium oscillations in the pedunculopontine nucleus. J Appl
825   Physiol (1985) 115, 1402–1414.
826   https://doi.org/10.1152/japplphysiol.00762.2013

827 Jellinger, K., 1988. The pedunculopontine nucleus in Parkinson's disease, progressive
828   supranuclear palsy and Alzheimer's disease. J Neurol Neurosurg Psychiatry 51,
829   540–543. https://doi.org/10.1136/jnnp.51.4.540

830 Johnson, S.W., Seutin, V., North, R.A., 1992. Burst firing in dopamine neurons induced

831   by N-methyl-D-aspartate: role of electrogenic sodium pump. Science 258,

832   665–667. https://doi.org/10.1126/science.1329209

833   Kang, Y., Kitai, S.T., 1990. Electrophysiological properties of pedunculopontine

834   neurons and their postsynaptic responses following stimulation of substantia

835   nigra reticulata. Brain Res 535, 79–95. https://doi.org/10.1016/0006-

836   8993(90)91826-3

837   Karachi, C., Grabli, D., Bernard, F.A., Tandé, D., Wattiez, N., Belaid, H., Bardinet, E.,

838   Prigent, A., Nothacker, H.-P., Hunot, S., Hartmann, A., Lehéricy, S., Hirsch, E.C.,

839   François, C., 2010. Cholinergic mesencephalic neurons are involved in gait and

840   postural disorders in Parkinson disease. J Clin Invest 120, 2745–2754.

841   https://doi.org/10.1172/JCI42642

842   Kezunovic, N., Urbano, F.J., Simon, C., Hyde, J., Smith, K., Garcia-Rill, E., 2011.

843   Mechanism behind gamma band activity in the pedunculopontine nucleus.

844   Eur J Neurosci 34, 404–415. https://doi.org/10.1111/j.1460-

845   9568.2011.07766.x

846   Liss, B., Striessnig, J., 2019. The Potential of L-Type Calcium Channels as a Drug Target

847   for Neuroprotective Therapy in Parkinson's Disease. Annu Rev Pharmacol

848   Toxicol 59, 263–289. https://doi.org/10.1146/annurev-pharmtox-010818-

849   021214

850   Mena-Segovia, J., Bolam, J.P., 2017. Rethinking the Pedunculopontine Nucleus: From

851   Cellular Organization to Function. Neuron 94, 7–18.

852   https://doi.org/10.1016/j.neuron.2017.02.027

853   Ortner, N.J., 2021. Voltage-Gated Ca2+ Channels in Dopaminergic Substantia Nigra

854   Neurons: Therapeutic Targets for Neuroprotection in Parkinson's Disease?

855   Front Synaptic Neurosci 13, 636103.

856   https://doi.org/10.3389/fnsyn.2021.636103

857   Parkinson Study Group STEADY-PD III Investigators, 2020. Isradipine Versus Placebo in

858   Early Parkinson Disease: A Randomized Trial. Ann Intern Med 172, 591–598.

859   https://doi.org/10.7326/M19-2534

860   Philippart, F., Destreel, G., Merino-Sepúlveda, P., Henny, P., Engel, D., Seutin, V., 2016.

861   Differential Somatic Ca2+ Channel Profile in Midbrain Dopaminergic Neurons.

862   J Neurosci 36, 7234–7245. https://doi.org/10.1523/JNEUROSCI.0459-16.2016

863   Ping, H.X., Shepard, P.D., 1996. Apamin-sensitive Ca(2+)-activated K+ channels

864   regulate pacemaker activity in nigral dopamine neurons. Neuroreport 7, 809–

865   814. https://doi.org/10.1097/00001756-199602290-00031

866   Poewe, W., Seppi, K., Tanner, C.M., Halliday, G.M., Brundin, P., Volkmann, J., Schrag,

867   A.-E., Lang, A.E., 2017. Parkinson disease. Nat Rev Dis Primers 3, 17013.

868   https://doi.org/10.1038/nrdp.2017.13

869   Puopolo, M., Raviola, E., Bean, B.P., 2007. Roles of subthreshold calcium current and
870   sodium current in spontaneous firing of mouse midbrain dopamine neurons. J
871   Neurosci 27, 645–656. https://doi.org/10.1523/JNEUROSCI.4341-06.2007

872   Rice, M.E., Cragg, S.J., Greenfield, S.A., 1997. Characteristics of electrically evoked
873   somatodendritic dopamine release in substantia nigra and ventral tegmental
874   area in vitro. J Neurophysiol 77, 853–862.
875   https://doi.org/10.1152/jn.1997.77.2.853

876   Rinne, J.O., Ma, S.Y., Lee, M.S., Collan, Y., Röyttä, M., 2008. Loss of cholinergic
877   neurons in the pedunculopontine nucleus in Parkinson's disease is related to
878   disability of the patients. Parkinsonism Relat Disord 14, 553–557.
879   https://doi.org/10.1016/j.parkreldis.2008.01.006

880   Rye, D.B., Saper, C.B., Lee, H.J., Wainer, B.H., 1987. Pedunculopontine tegmental
881   nucleus of the rat: cytoarchitecture, cytochemistry, and some extrapyramidal
882   connections of the mesopontine tegmentum. J Comp Neurol 259, 483–528.
883   https://doi.org/10.1002/cne.902590403

884   Sabatini, B.L., Oertner, T.G., Svoboda, K., 2002. The life cycle of Ca(2+) ions in
885   dendritic spines. Neuron 33, 439–452. https://doi.org/10.1016/s0896-
886   6273(02)00573-1

887   Sébille, S.B., Rolland, A.-S., Faillot, M., Perez-Garcia, F., Colomb-Clerc, A., Lau, B.,
888   Dumas, S., Vidal, S.F., Welter, M.-L., Francois, C., Bardinet, E., Karachi, C.,
889   2019. Normal and pathological neuronal distribution of the human
890   mesencephalic locomotor region. Mov Disord 34, 218–227.
891   https://doi.org/10.1002/mds.27578

892   Shin, J., Kovacheva, L., Thomas, D., Stojanovic, S., Knowlton, C.J., Mankel, J., Boehm,
893   J., Farassat, N., Paladini, C., Striessnig, J., Canavier, C.C., Geisslinger, G.,
894   Roeper, J., 2022. Cav1.3 calcium channels are full-range linear amplifiers of
895   firing frequencies in lateral DA SN neurons. Sci Adv 8, eabm4560.
896   https://doi.org/10.1126/sciadv.abm4560

897   Surmeier, D.J., Guzman, J.N., Sanchez-Padilla, J., 2010. Calcium, cellular aging, and
898   selective neuronal vulnerability in Parkinson's disease. Cell Calcium 47, 175–
899   182. https://doi.org/10.1016/j.ceca.2009.12.003

900   Surmeier, D.J., Nguyen, J.T., Lancki, N., Venuto, C.S., Oakes, D., Simuni, T., Wyse, R.K.,
901   2022. Re-Analysis of the STEADY-PD II Trial-Evidence for Slowing the
902   Progression of Parkinson's Disease. Mov Disord 37, 334–342.
903   https://doi.org/10.1002/mds.28850

904   Takakusaki, K., Kitai, S.T., 1997. Ionic mechanisms involved in the spontaneous firing
905   of tegmental pedunculopontine nucleus neurons of the rat. Neuroscience 78,
906   771–794. https://doi.org/10.1016/s0306-4522(96)00540-4

907   Wilson, C.J., Callaway, J.C., 2000. Coupled oscillator model of the dopaminergic

908   neuron of the substantia nigra. J Neurophysiol 83, 3084–3100.

909   https://doi.org/10.1152/jn.2000.83.5.3084

910